Structure Optimization of Au Wire Wedge-bond for High Temperature Applications

Shun-Tien (Ted) Lin,[1] Xiaodong Luo,[2] and Liang-Yu Chen[3]
[1]Hamilton-Sundstrand Corp, Windsor Locks, CT 06096
[2]United Technologies Research Center, East Hartford, CT 06108
[3]Ohio Aerospace Institute/NASA Glenn Research Center, Cleveland, OH 44135

Abstract

Thermo-mechanical performance of wirebonds is critical to the reliability of electrical interconnection systems of chip-level packaging for high temperature electronics because these devices are subject to a much wider temperature range compared with that for conventional electronics. The thermo-mechanical stress in wirebonds due to thermal expansion (CTE) mismatch between the metal wire, bond pads, chip and substrate materials may cause degradation and failure of wirebonds. The most common failure mode of wirebonds is delamination/cracking at wire/bond-pad and bond-pad/chip (or substrate) interfaces. A parametric study of the thermo-mechanical reliability of gold (Au) wire wedge-bonds by nonlinear finite element analysis (FEA) is conducted in order to establish a tool to optimize the thermo-mechanical performance of Au wirebonds for high temperature applications. A Au wire wedge-bond composed of 1 mil diameter Au wire bonded to Au bond pad on a 96% Al_2O_3 substrate is examined. Temperature dependent elastic material properties of Au and alumina are used for stress/strain assessment at potential failure locations. The stresses/strains at potential failure locations resulting from 2D FEA simulations are coupled with a multi-parameter numeric optimization tool. These stresses are then minimized through adjustments of wire geometry, bond pad thickness, and dimensions of 'toe' and 'heel' on bond pads to optimize the thermal reliability of Au wire wedge-bonds. 2D FEA simulation is run using temperature dependent Au elastic-plastic properties to determine plastic strain distribution of the optimized structure for reliability assessment.

Introduction

Wire bonds in a microelectronic package provide electrical connections between the chip and the leads or I/Os of a package. For conventional electronics operating between -30 and 150°C, failure of the wire bond occurs predominantly as a result of thermo-mechanical fatigue caused by (1) shear stress generated between the bond pad and the (wedged) wire, (2) repeated flexure of the wire, and (3) shear stress generated between the bond pad and the substrate. These stresses are due to the mismatch of CTEs of metal (wire and bond pads) and substrate materials, and residual stress from the bonding process. The dominant failure mechanism depends on the operating environment, the wire and bond pad materials, and the geometry of the wire and the wire bond. Wire bonds are subject to significant stresses during operation as a result of temperature and power cycling. Operational wire bond failures account for 25-30% of the package failures in the conventional temperature range [1].

Pecht et al [1, 2] developed a closed-form failure prediction model for each failure mechanism. Wen [3] analyzed stress levels in wire bonds for a power electronics module using three-dimensional elastic-plastic finite element approach. However, no fatigue life model was presented using deformation-based theory for the aluminum wire bonds.

For high temperature electronics and sensors, the temperature range to which the devices are exposed to is much wider [4] compared with that for conventional electronics. Thus the thermal stress due to CTEs mismatch (between the substrate/die materials and wire material) is anticipated to be much higher than that for conventional electronics application. Therefore, it is meaningful to create a numerical tool to assess the stress levels in wirebonds of various materials and bond structures/methods in order to optimize the thermal reliability of wirebonds through minimization of the thermal stress. This tool would help us to design the geometry of the wire-span, select the bond format, select the substrate and wire materials, and assess the reliability of the optimized wirebonds. This paper discusses finite element analysis (FEA) based geometric optimization of a 1 mil Au wire wedgebond to Au thick-film metallization on 96% alumina substrate and assessment of maximum plastic strains of the wirebond at 500°C during the first thermal cycle. The stress and strain resulting from FEA simulation are coupled to a multi-parameter numerical optimization tool based on a Sequential Quadratic Programming Method, which minimizes the stress at potential failure locations. The stresses selected for optimization are maximum bending strain of the wire, maximum shear strain between the wire and

bond pad, and maximum shear strain between the bond pad and the substrate. The wirebond geometry includes the length and shape of the wire, the dimensions of 'toe' and 'heel' of wirebonds on the bond pads, and the thickness of the bond pads.

FEA Model

The 1 mil diameter Au wire was wedge-bonded on two identical Au thick-film bond pads. The wire and wirebond assembly is assumed to be symmetric with respect to a central symmetry line. The length of both wedge-bonds is 100 micro-meter (µm). The thickness of the 96% alumina substrate is 625 µm (25 mil), and the substrate length is 10 times the distance between two wirebonds (from heel to heel). The Au wire is assumed to be composed of a
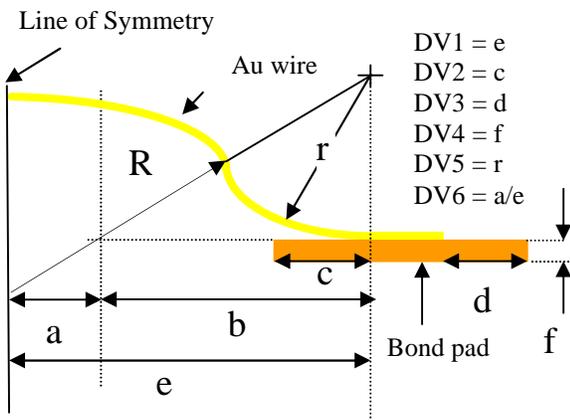
Figure 1: Six-parameter geometry model for wirebond interconnection loop FEA and geometry optimization.

flat bonded section (100 µm), a circular section (with radius r) which is tangential to the flat bonded section at its 'heel', a second circular section (with radius R) which is tangential to the first circular section at a turning point, as shown in Figure 1. The geometry of the wire and bonds is described using the following six variables (see Figure 1), DV1-6: DV1 is a half of the distance between wire bonds (from heel to heel), DV2 is the bond pad length on the left side of the wire bond ('heel') shown in the figure, DV3 is the bond pad length on the right side of wire bond ('toe'), DV4 is the bond pad thickness, DV5 is the radius of the first circular section of the wire, DV6 is a geometric parameter that defines, along with DV1 and DV5, the radius of the second circular section of the wire (controls both the angle span between two turning points of the wire and the angle span of the first circular section, see Figure 1). Figure 2a-d show finite element meshes of the wire bond for four different initial sets of design values (DV1-6). The Table 1 shows four sets of the initial design variables shown in Figure 2a-d.

It is assumed that the wire is ideally bonded to bond pads and the bond pads are also ideally bonded to the substrate so all the displacements at the Au-wire/Au-bond-pad and Au-pad/substrate interfaces are continuous. The assembly is subjected to a 25°C to 500°C temperature excursion. The ANSYS parametric finite element model is developed using ANSYS Parametric Design Language (APDL).
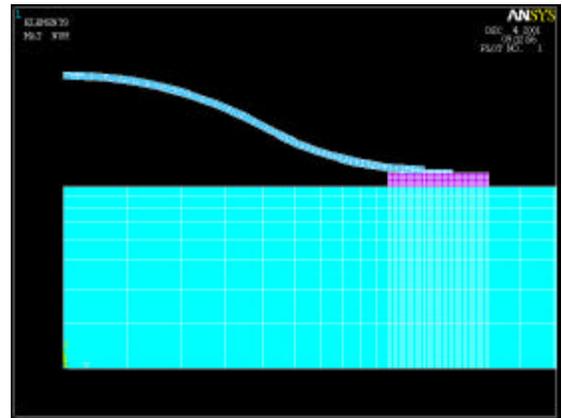
Figure 2a: ANSYS finite element 2D mesh of wire bond (DV set 1).
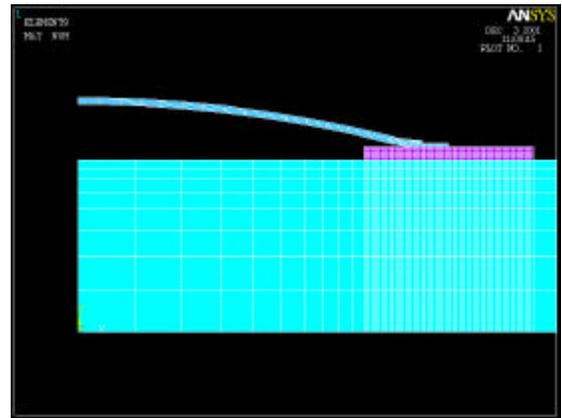
Figure 2b: ANSYS finite element 2D mesh of wire bond (DV set 2).

Material Properties

Temperature dependent linear elastic properties of 96% Al_2O_3 substrate and gold (for both wire and gold thick-film bond pads) [5] are used for FEA simulation of stress and strain distributions of a given geometry configuration and to identify the locations of potential failure at 500°C. Both maximum stresses and failure locations are dependent on the geometry (DV1-6) of the wire and wirebond. After optimization of the geometry of the wire and wirebond, temperature dependent elastic-plastic properties of Au are used for plastic strain

simulation at various potential failure locations for reliability assessment [6].
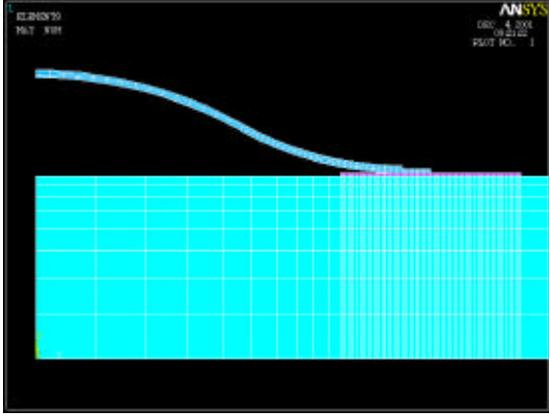
Figure 2c: ANSYS finite element 2D mesh of wire bond (DV set 3).
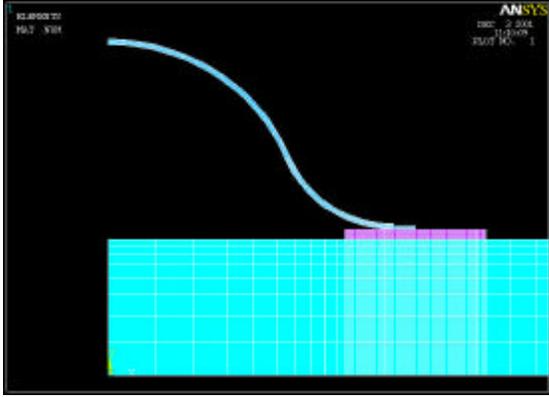
Figure 2d: ANSYS finite element 2D mesh of wire bond (DV set 4).

Table 1: 4 sets of the initial design variables shown in Figure 2a-d.

Design Variable Sets	Set1	Set2	Set3	Set4	ABAQUS
DV1 (mils)	50.8	50.1	50.1	50.1	50
DV2 (mils)	5	8.48	8.48	8.48	4
DV3 (mils)	5	12.35	12.35	12.35	4
DV4 (mils)	2	2	2	0.5	2
DV5 (mils)	44.96	20	20	45	46
DV6	0.5	0.1	1	0.5	0.44

Optimization and Algorithm

The way to optimize a wire bond interconnection loop is to minimize the stresses (or strains) at potential failure locations, while satisfying the parametric constraints of the wire bond system, as described later. The optimization problem of the wire bond interconnection loop can be formulated as: Minimize the strain ε at a potential failure location

$$\mathbf{e}(X) = F(X_1, X_2, X_3, X_4, X_5, X_6) \quad (1)$$

$X_{1, 2, 3}$ are subject to geometry constraints:

$$X_2 \leq X_1$$
$$X_3 \leq 9X_1 - 0.003937 \quad (2)$$

and X_{1-6} are subject to the constraints of upper and lower limits:

$$X_i^L \leq X_i \leq X_i^U \quad (3)$$

where $X_1, X_2, X_3, X_4, X_5, X_6$ are the design variables (DV1-6) as defined in Figure 1, X_i^L and X_i^U are the lower and upper bounds of the design variables defined in Table 2. The optimization problem defined by Equations (1) ~ (3) can be solved by using any of the following algorithms: feasible direction method, sequential linear programming method, and sequential quadratic programming method. In this work, Sequential Quadratic Programming Method [7, 8], commonly called recursive quadratic programming method, is used to minimize the stress(es) at potential failure location(s). Although this is a comparatively complicated method, it has been found to be quite powerful if reasonable care is taken in formulating the optimization problem. The basic concept is to find a search direction S in parametric (X) space that will minimize a quadratic approximation to the Lagrangian function subject to linear approximations to the constraints. That is to find a vector S in X space that will minimize:

$$Q(S) = F(X^0) + \nabla F(X^0)^T S + S^T HS / 2 \quad (4)$$

S is generally subject to constraints of

$$\nabla g_j(X^0)^T S + \mathbf{g}g_j(X^0) \leq 0, \quad j = 1, ..., J \quad (5)$$

$$\nabla h_k(X^0)^T S + h_k(X^0) = 0, \quad k = 1,...,K \quad (6)$$

where H is the Hessian matrix (or its approximation) of $F(X)$ in X space, T is the matrix transposing operator. ∇ is the gradient operator in X space. X^o is the initial vector composed of X_i^o (i=1,…, 6). $\boldsymbol{g}$ is the parameter used to avoid or overcome constraint violations. g_j is the jth function of equality constraint, and h_k is the kth function of inequality constraint. J is the total number of equality constraints (in our case $J = 0$) and K is the total number of inequality constraints (in our case $K = 8$). This is a quadratic programming sub-problem which may be solved using standard quadratic methods [9].

Once the search direction is available, the exterior penalty function used to determine the step along S in parameter space can be minimized by solving a one-dimensional search problem:

$$\Phi = F(X) - \sum_{j=1}^{J} \boldsymbol{l}_j \min(0, g_j(X)) + C\sum_{k=1}^{K} \boldsymbol{l}_k |h_k(X)|^2 \quad (7)$$

where $\boldsymbol{l}_j$ are the Lagrangian multipliers from the quadratic subproblem and C is a positive constant.

Results
Optimization

Maximum bending strain of the wire (OBJ1), maximum shear strain at the interface between the wire and bond pad (OBJ2), and maximum shear strain at the interface between the bond pad and the substrate (OBJ3) are selected as

Table 2: Limits of design variables used in optimization process.

Design Variables	Lower Limit	Initial Value	Upper Limit
DV1 (mils)	5	50	100
DV2 (mils)	5	5	100
DV3 (mils)	5	10	300
DV4 (mils)	0.5	1	2
DV5 (mils)	20	45	100
DV6	0.1	0.5	1

objective functions in the optimization process. The limits and initial values of the design variables are listed in Table 2. Two constrains are also imposed on DV1, DV2, and DV3 in the optimization process: DV2 is always less than DV1, and DV3 is always less than nine times of DV1. The optimized results are listed in Table 3 for each objective function.

Table 3 shows the optimization results. The highlighted strains are the minimized maximum

strains when the objective functions are minimized individually and independently. The shear strain between bond pad and substrate is the highest after the OBJ1 and OBJ2 are minimized individually and independently. Physically, a joint at hetero-material interface is the most likely thermomechanical failure location, especially at high temperature. Therefore, highest priority is given to optimizing OBJ3.

Table 3: Optimization results.

Design Variables	OBJ1	OBJ2	OBJ3	Combined
DV1 (mils)	100	50.0842	50.098	100
DV2 (mils)	5	5	8.47762	8.307
DV3 (mils)	5	5	12.3457	12.25
DV4 (mils)	2	2	0.5	0.6782
DV5 (mils)	100	44.9578	45	24.073
DV6	1	0.5	0.5	0.504
Bending strain (wire)	2.06E-04	(5.45E-04)	(5.66E-04)	2.16E-04
Shear strain (wire/pad)	(3.31E-03)	3.32E-03	(4.002E-03)	4.00E-03
Shear strain (pad/sub)	(6.165E-03)	(6.165E-03)	4.01E-03	4.01E-03

The last column in Table 3 shows the optimal results when all three objective functions (the three strains) are minimized in a sequence based on the criticality of the strain components. The shear strain between pad and substrate is first minimized with the other two strains set free. Then the shear strain between wire and pad is optimized with an additional constraint that the shear strain between bond pad and the substrate be less or equal to its minimized value, while the wire bending strain is set free. This yields identical optimization results for the two strains as if they are individually and independently optimized, indicating that the maximum shear strain at wire/pad interface is highly and positively correlated to that at bond-pad/substrate interface. Finally the wire bending strain is minimized with the other two strains constrained not to exceed their sequentially optimized values. The final optimization result listed in the last column of Table 3 gives an optimized design of the wire bond system that produces reduced strain levels. The ABAQUS finite element mesh is shown in Figure 3.

Plastic Deformation

Material properties of gold wire and gold thick-film were the same as those we reported earlier [6]. Temperature dependent elasticity and plasticity are used to simulate the maximum plastic strain (EPS) distribution of the optimized wirebond. The initial design variable set for this model is listed in Table 1.

Figure 4a and b show the finite element analysis results of maximum EPS. Maximum EPS is estimated to be 7.8515E-03 inside the bond pad in the area close to the bond pad/substrate interface. The maximum EPS in the wire is 3.83261E-03 in the area close to the bond 'heel'. Maximum shear EPS at the bond-pad/substrate interface can be as high as 2.13E-02. This EPS might be significantly reduced via shrink the size of the bond pads (release the lower bond of the heel).

Compared with the plastic strains of Au thick-film based SiC die-attach with 1 mm x 1 mm SiC die on alumina and aluminum nitride substrates [6], the crack initiation life for wire bond system is expected to be much longer. Therefore, it is expected that the Au 1 mil diameter Au wire and wirebond interconnection loops should be more reliable.
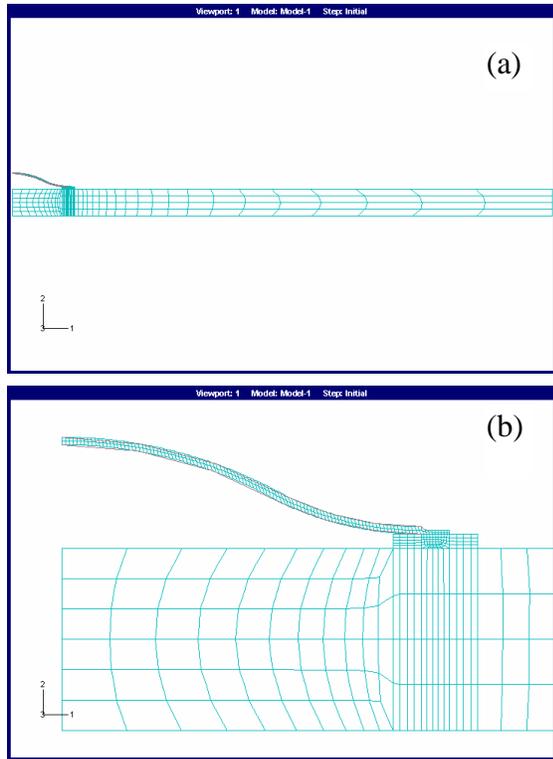
Figure 3: ABAQUS finite element mesh of wire bond (a) half model (b) close-up view.

Summary and Discussions

An introductory FEA based numeric tool for optimization of geometry of wirebond interconnection loops for high temperature operation is demonstrated. The maximum bending strain of the wire, maximum shear strain between the wire and bond pad, and maximum shear strain between the bond pad and the substrate are first assessed using FEA with temperature dependent elastic properties of

substrate and Au. The FEA results of these strains are coupled to a sequential numerical optimization tool. A Sequential Quadratic Programming Method is used to sequentially minimize all three stresses at potential failure locations to generate an optimized geometry design of the wirebond interconnection loop. Following that, FEA with temperature dependent elastic-plastic Au material property is used for simulation of EPS at potential failure locations for reliability assessment of 1 mil Au wirebonds on alumina substrate. The wirebond interconnection system should be more reliable than the SiC die-attach assembly (with 1 mm x 1 mm SiC die)
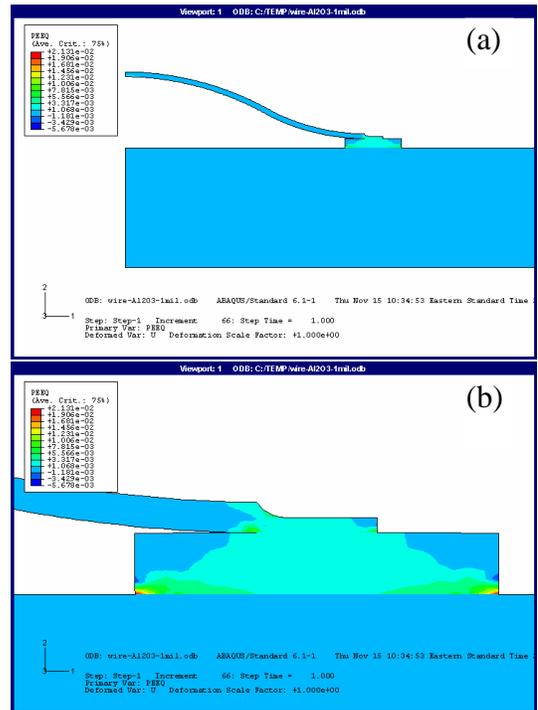
Figure 4: Equivalent plastic strain distributions: (a) half model (b) blow-up view of wirebond.

reported earlier [6].

Elastic shear strain between bond pad and substrate (simulated using temperature dependent elastic Au property) is slightly higher than that between wire and bond pad (based on the stress distribution results using elastic Au property), as shown in Table 3. So it is not obvious from the stress distribution which failure mechanism is dominant for this case. However, the EPS results of FEA using temperature dependent elastic-plastic properties of Au show that the failure would start from the corner at the interface between the bond pads and substrate. The EPS at the interface might be significantly reduced by shrinking the pad size (releasing the lower bond of DV3). The ultimate failure

mechanism would depend on the thermal profile and the adhesion strength of the bond pads on the ceramic substrate, which has not been quantitatively determined.

This FEA based optimization tool can also help packaging designers to select substrate and wire materials and bonding methods/structure (wedge-bond vs. ball-bond) for optimized performance in a wide temperature range. The plastic deformation of wire and wirebonds generated in the wedge-bonding process at $150^{o}C$ is not considered in FEA simulation of stress(es) and strains in this work. The plastic strain resulting from wedge-bonding very likely is dominant compared with thermal plastic strains. However, it is reported that atomic diffusion of Au becomes very active at temperatures close to $600^{o}C$ [10] so it is anticipated that thermal stress in Au might be largely relaxed at $500^{o}C$ via atomic diffusion of Au. Effects of electrical migration on thermomechanical failure are proportional to the density of DC current, so for low power circuits they might be ignored in reliability assessment in dynamic thermal environments.

REFERENCES

1. M. Pecht, P. Lall, and A.Dasgupta, *A Failure Prediction Model for Wire Bonds*, Proc. of the 1989 Intl. Symp. On Hyb. Micro., 1989, pp. 607-613.
2. M. Pecht, P.Lall, and S.J. Whelan, *Temperature Dependence of Microelectronic Device Failures*, Quality and Reliability Engineering International, vol. 6, Sept.-Oct. 1990, pp. 275-284.
3. S. Wen, *Thermal and Thermo-Mechanical Analyses of Wire Bond vs. Three-Dimensionally Packaged Power Electronics Modules*, MS Thesis, Virginia Polytech Institute State University, December 16, 1999.
4. F.P. McCluskey, R. Grzybowski, and T. Podlesak, High Temperature Electronics, CRC Press, Boca Raton, 1996.
5. L.-Y. Chen and J.-F. Lei, *Packaging of Harsh-Environment MEMS Devices*, CRC MEMS Handbook, Boca Raton, LA, October, 2001.
6. S.-T. Lin and L.-Y. Chen, *Thermo-Mechanical Optimization of a Gold Thick-film based SiC Die-attach Assembly using Finite Element Analysis*, Proceedings of the 6th International High Temperature Electronics Conference (6th HiTEC), Albuquerque, NM, June 2-5, 2002.
7. G. N. Vanderplaats and F. Moses, *Structural Optimisation by Methods of Feasible Directions*, *Journal of Structural Division*, ASCE, No. ST3, pp. 671 – 690, March 1972.
8. G.N. Vanderplaats, *Mathematical Programming Methods for Constrained Optimisation: Primal Methods*, Structural Optimisation: Status and Promise, Manohar P. Kamat edited, Vol. 150, Progress in Astronautics and Aeronautics, A. R. Seebass editor-in-chief, AIAA Inc. 1993.
9. P.B. Thanedar, J. Arora, , C.H. Tseng, O.K. Lim, and G.J. Bark, *Performance of Some SPQ Algorithms on Structural Design Problems*, International Journal of Numerical Methods in Engineering, Vol. 23, No. 3, pp. 2187 – 2230, 1986.
10. L.-Y. Chen, G.W. Hunter, and P. G. Neudeck, *Silicon Carbide Die Attach Scheme for $500^{o}C$ Operation*, Vol. 622, Material Research Society (MRS), pp. T8.10.1-6, 2000.

Biography

Liang-Yu Chen received his Ph.D. degree in experimental condensed matter physics from Case Western Reserve University, Cleveland, OH, in 1994. After graduation, he joined the NASA Glenn Research Center, Cleveland, as a National Research Council Research Fellow studying surface and interface stability of silicon carbide high temperature chemical sensors. Currently he is a senior scientist at the Ohio Aerospace Institute working on the high temperature electronics packaging program at NASA Glenn Research Center. His current research interests include advanced packaging materials and interfacial properties for high temperature and other harsh environment applications.